

DETECTION OF A WHITE DWARF COMPANION TO THE WHITE DWARF SDSSJ125733.63+542850.5

T.R. MARSH, B.T. GÄNSICKE, D. STEEGHS

Department of Physics, University of Warwick, Coventry CV4 7AL, UK

J. SOUTHWORTH

Astrophysics Group, Keele University, Keele, Staffordshire ST5 5BG, UK

D. KOESTER

Institut für Theoretische Physik und Astrophysik, University of Kiel, 24098 Kiel, Germany

V. HARRIS

133 Jackman Close, Abingdon, Oxfordshire OX14 3GB, UK

L. MERRY

Flat 4, 8 The Lakes, Larkfield, Kent ME20 6GE, UK

Draft version October 26, 2018

ABSTRACT

SDSSJ125733.63+542850.5 (hereafter SDSSJ1257+5428) is a compact white dwarf binary from the Sloan Digital Sky Survey that exhibits high-amplitude radial velocity variations on a period of 4.56 hours. While an initial analysis suggested the presence of a neutron star or black-hole binary companion, a follow-up study concluded that the spectrum was better understood as a combination of two white dwarfs. Here we present optical spectroscopy and ultraviolet fluxes which directly reveal the presence of the second white dwarf in the system. SDSSJ1257+5428's spectrum is a composite, dominated by the narrow-lined spectrum from a cool, low gravity white dwarf ($T_{\text{eff}} \simeq 6300$ K, $\log g = 5$ to 6.6) with broad wings from a hotter, high-mass white dwarf companion (11,000 to 14,000 K; $\sim 1 M_{\odot}$). The high-mass white dwarf has unusual line profiles which lack the narrow central core to H α that is usually seen in white dwarfs. This is consistent with rapid rotation with $v \sin i = 500$ to 1750 km s^{-1} , although other broadening mechanisms such as magnetic fields, pulsations or a helium-rich atmosphere could also be contributory factors. The cool component is a puzzle since no evolutionary model matches its combination of low gravity and temperature. Within the constraints set by our data, SDSSJ1257+5428 could have a total mass greater than the Chandrasekhar limit and thus be a potential Type Ia supernova progenitor. However, SDSSJ1257+5428's unusually low mass ratio $q \approx 0.2$ suggests that it is more likely that it will evolve into an accreting double white dwarf (AM CVn star).

Subject headings: supernovae: general – white dwarfs – accretion – binaries: close

1. INTRODUCTION

Close pairs of white dwarfs with combined masses greater than the Chandrasekhar limit have long been discussed as potential progenitors of Type Ia supernovae (Iben & Tutukov 1984; Webbink 1984). However, despite searches, (Robinson & Shafter 1987; Bragaglia et al. 1990; Marsh et al. 1995; Napiwotzki et al. 2003) no secure examples of double white dwarfs both massive enough and short-period enough to merge within a Hubble time have been found. Only about 1 in a 1000 white dwarfs are required to be in such systems to match Type Ia rates (Nelemans et al. 2001b). Since only of order 1000 white dwarfs have been searched for binarity to date, the deficit is not yet significant, however it continues to be worth searching for more such systems. In an effort to do so we examined the spectra of DA white dwarfs (those showing

spectra with hydrogen absorption only) from the SDSS survey (Eisenstein et al. 2006), looking for objects of discrepant radial velocity. One star, SDSSJ1257+5428 was an obvious outlier with a mean radial velocity of -300 km s^{-1} . In this paper we present follow-up spectroscopy to elucidate the nature of this object.

SDSSJ1257+5428 was the subject of a similar study by Badenes et al. (2009). They found that it was a binary, measured a radial velocity semi-amplitude of $K_1 = 323 \pm 6 \text{ km s}^{-1}$ on a period of 4.56 hours and fitted their spectra with a white dwarf of temperature ~ 9000 K and high mass, $\sim 0.9 M_{\odot}$. The period, radial velocity amplitude and white dwarf mass give a minimum mass for the companion of $1.6 M_{\odot}$, suggesting that it is either a neutron star or black-hole. Badenes et al. (2009) estimated a distance of 48 pc for SDSSJ1257+5428, implying that such systems may be rather common.

Badenes et al. (2009) recognised that their spectral fits were problematic, and in particular failed to fit the nar-

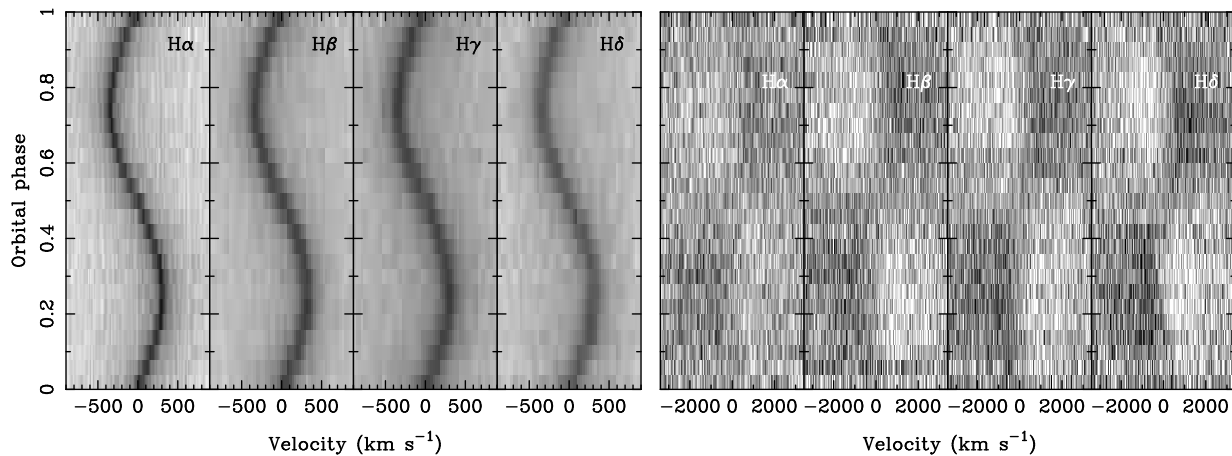


FIG. 1.— The panels show phase-folded trailed spectra of the first four Balmer lines of SDSSJ1257+5428, $H\alpha$ – δ , left to right. The left-hand panel shows the raw data; the right-hand panel, which shows the data after removal of the primary’s motion and mean spectrum, reveals anti-phased features from the massive secondary white dwarf. (Note the change of horizontal scale between the two panels.)

row cores of the Balmer lines. Thus while they favored a neutron star or a black-hole for the companion, they could not entirely eliminate the possibility that it was another white dwarf. Kulkarni & van Kerkwijk (2010) took three high signal-to-noise spectra which showed asymmetries suggesting exactly this; they showed that their spectra could be fit by a combination of a cool, low mass white dwarf (6250 ± 250 K, $0.15 \pm 0.05 M_{\odot}$) plus a hotter, massive white dwarf companion ($13,000 \pm 800$ K, $0.92 \pm 0.13 M_{\odot}$).

Kulkarni & van Kerkwijk (2010)’s paper appeared shortly after the original submission of our work. Although both our papers agreed upon the basic double white dwarf nature of SDSSJ1257+5428, there were significant differences of detail, with inconsistencies in both masses and temperatures. In an effort to understand these, we have since carried out additional fits to our data, which we present here along with our original approach. In addition, an improved *Swift* calibration has given us more confidence in the modelling of the UV-optical spectral energy distribution. Our new results agree more closely with Kulkarni & van Kerkwijk (2010) than our original analysis, but also reveal uncertainties in the system properties which make it impossible to establish securely such fundamental properties as whether the system is super-Chandrasekhar or not. We begin with a description of our observational material.

2. OBSERVATIONS AND REDUCTION

We obtained 140 spectra in the *B* and *R* bands covering the Balmer series on the William Herschel Telescope in La Palma using the ISIS double-beam spectrograph. The first 22 spectra were taken in service mode on the night of April 20, 2008, while the final 118 were acquired during a four night run spanning April 29 to May 2, 2009. The data were debiased, flat-fielded and optimally extracted (Horne 1986; Marsh 1989). The wavelength scale for each spectrum was linearly interpolated in time from pairs of bracketing arc calibration spectra. In 2008, the night was clear with seeing 0.8 to 1.6 arcsec, however the Moon was full. In 2009, the Moon was only 40% illuminated, but conditions were poorer, and we lost a total of one night to clouds while the seeing varied from 1.0 to 2.5 arcsec.

In addition to the optical spectroscopy, we obtained ultraviolet flux measurements of SDSSJ1257+5428 with

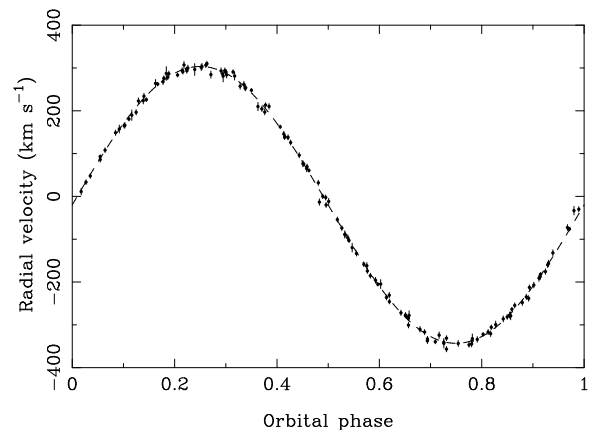


FIG. 2.— Radial velocities of $H\alpha$ from 2008 and 2009 folded on the ephemeris of this paper.

the *Swift* satellite and accessed additional archival data from 7 epochs of observations covering the interval Aug 24 2009 – Jan 13 2010. Our summed images had effective exposure times ranging from 818 to 5608s. SDSSJ1257+5428 was well detected in all four UV filters provided by *Swift*/UVOT (Romig et al. 2005). Aperture photometry with a 5” extraction region and an annular sky region was performed using the SWIFT data analysis package V3.7 within the HEASoft V6.10 release. Associated zero-point calibration files and filter effective area curves (Jan 2011 release) were used to calculate the fluxes for each filter.

3. RESULTS

In all that follows we will refer to the component most obvious in the spectra as the primary star, and its companion as the secondary star. This means that the primary star is low mass and cool, while the secondary star is high mass and hot.

3.1. The primary star

Orbital motion of large amplitude was immediately apparent in the spectra. The left panel of Fig. 1 shows phase-folded trailed spectra of the first four Balmer lines displaying high-amplitude orbital motion and an apparently single-lined binary star.

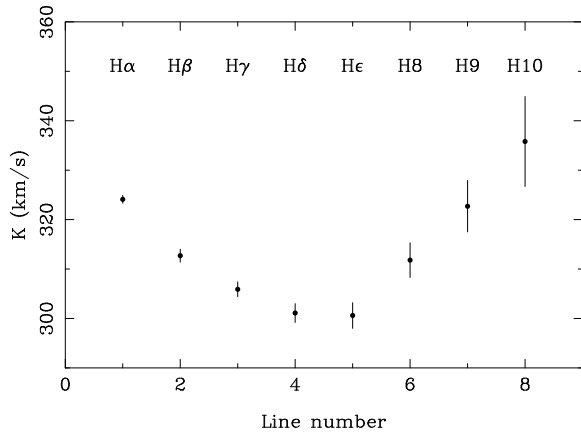


FIG. 3.— The radial velocity semi-amplitude of SDSSJ1257+5428 from H α to H10 showing the varying influence of the companion (which always reduces the amplitude) across the Balmer series.

We fitted the radial velocities (Fig. 2) of the Balmer lines using combinations of 3 Gaussians for each line, with full width half maxima (FWHM) and depths optimised to minimise χ^2 . Given the large radial velocity amplitude of SDSSJ1257+5428, the four night run in 2009 was sufficient to extrapolate back to the service night of a year earlier to find a unique alias, leading to the following ephemeris (on a UTC timescale corrected for light-travel time to the heliocentre):

$$HJD = 2454846.17470(8) + 0.18979154(9)E, \quad (1)$$

where the time of zero phase corresponds to the time when the primary star is closest to Earth. While our period is consistent with that of Badenes et al. (2009) ($P = 0.18979(3)$ days), our zero phase is not, since on our ephemeris their zero phase occurs at $E = 115.619 \pm 0.004$; this is the result of an error of 0.5 days in the calculation of Julian Days together with no allowance for light travel time in Badenes et al. (2009) (C.Badenes, priv. comm.); we have in addition confirmed that our ephemeris correctly predicts the velocities of the SDSS spectra which were taken in 2003.

Having established a unique period alias, from now on we use only the 2009 data because of differences in the instrumental setups between 2008 and 2009 which make consistent continuum fitting difficult. Sinusoidal fits were made to the radial velocities measured for each Balmer line from H α to H10. The semi-amplitudes were seen to vary from $324.1 \pm 0.8 \text{ km s}^{-1}$ for H α to $300.6 \pm 2.6 \text{ km s}^{-1}$ for H ϵ , rising again in the higher Balmer lines (Fig. 3). The variation from line to line is a symptom of the presence of a second broad-lined white dwarf. As indicated earlier, and as will be seen later, the secondary white dwarf is hotter and more massive than the primary. Therefore, owing to its temperature on the one hand, and its high gravity on the other, the secondary is expected to contribute relatively weakly at H α and in the higher Balmer series, but more strongly in intermediate series lines. This is exactly what is seen in Fig. 3, with the radial velocity semi-amplitude acting as a proxy for the relative line strength from the two components.

3.2. The secondary star

To search for more direct signs of a companion we first fitted and normalised the continua of the spectra

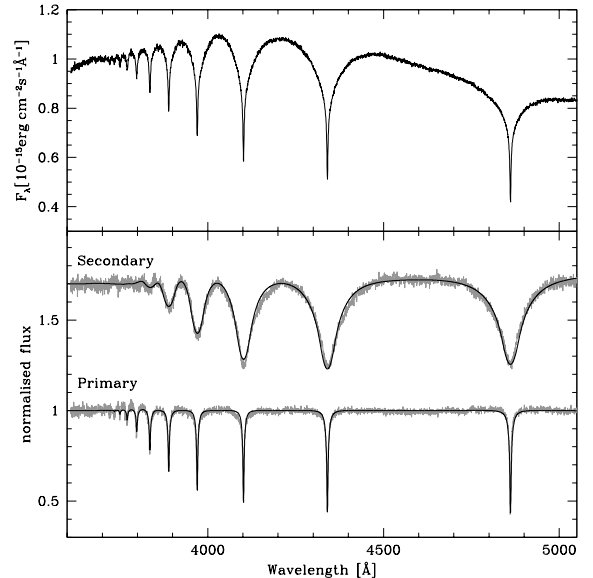


FIG. 4.— The average B -band spectrum (top) and results of disentangling the spectra of SDSSJ1257+5428 (gray lines) along with model atmospheres (primary: $T_{\text{eff}} = 6900 \text{ K}$, $\log g = 6.75$; secondary: $T_{\text{eff}} = 10300 \text{ K}$, $\log g = 8.70$) for a light ratio of 0.7 (section 3.4) and $v \sin i = 1500 \text{ km s}^{-1}$ (black lines). For disentangling, the radial-velocity semi-amplitudes were fixed at $K_1 = 330 \text{ km s}^{-1}$ and $K_2 = 100 \text{ km s}^{-1}$, but the results were insensitive to the precise value of K_2 .

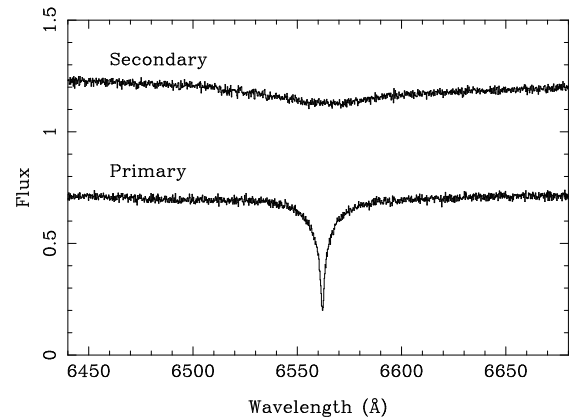


FIG. 5.— The disentangled H α spectra with the secondary star component plotted at the top. As with Fig. 4, the continuum levels are indeterminate.

between the Balmer lines. Next we shifted out the primary star’s orbital motion and subtracted the average of the resulting spectra. If only one component contributes significantly, this procedure should leave only noise. Any contribution from a secondary star will cause correlations amongst the residuals. The right-hand panel of Fig. 1 shows such residuals which moreover are anti-phased compared to the left-hand panel. This is the signature of a second contributing white dwarf, albeit distorted by the subtraction process.

The spectra of two stars within a binary can also be recovered using a method applied successfully to main-sequence binaries known as “disentangling” (Simon & Sturm 1994). Although the broad absorption lines of white dwarfs make it harder to establish the reliable normalisation required for disentangling, we tried it out to see if any separation of the two spectra was possi-

ble. Its appeal is that it requires no *a priori* assumptions concerning the spectra of the two components, although it cannot return the individual continua, and takes as input continuum-normalised spectra. The results for the blue spectra, plotted in Figs 4, and over-plotted with model atmospheres, show a pair of low- and high-gravity white dwarf spectra. The high-gravity secondary contributes the broad line wings and it is thus clear why Badenes et al. (2009) over-estimated the mass of the primary and had difficulties obtaining good spectral fits. The process of disentangling leaves the continuum levels undetermined; we discuss the model atmosphere fits further in section 3.4. The disentangled $H\alpha$ profiles (Fig. 5) are remarkable for an absence of any sharp line core in the high gravity spectrum. $H\alpha$ lines in white dwarfs of this temperature usually display a sharp dip at the line centre 2 or 3 Å in width as the result of non-LTE effects (Greenstein & Peterson 1973; Koester & Herrero 1988; Heber et al. 1997), but Fig. 5 shows no sign at all of this. The figure also makes it clear why $H\alpha$ relatively faithfully traces the motion of the primary.

3.3. Mass constraints

We were unable to obtain a reliable direct measurement of the semi-amplitude of the secondary star K_2 from our data, a consequence, we believe, of its high gravity and the absence of any sharp line cores, combined with the difficulty of defining reliable continua. However, when trying to obtain simultaneous fits to both stars, we found that the extra freedom of a secondary component always allowed K_1 to increase above the directly-fitted values to a value consistently close to $330 \pm 2 \text{ km s}^{-1}$ which we take to be the true value of K_1 . The directly measured values are biased towards lower values by the contribution from the secondary, although as Fig. 3 demonstrates, the effect is relatively slight in $H\alpha$ and in the higher Balmer series where the secondary star’s high gravity ensures that it contributes little. The value of K_1 , along with the presence of a second white dwarf leads to the mass constraints plotted in Fig. 8.

3.4. Spectroscopic fits

Our WHT data reveal that the narrow Balmer lines in SDSSJ1257+5428 extend up to H12 (Fig. 4), implying unambiguously that the cooler white dwarf (primary) is of an unusually low surface gravity. In the original submission of this paper, we modelled our WHT spectroscopy of SDSSJ1257+5428 as we describe in Sect. 3.4.1, finding that SDSSJ1257+5428 is composed of a very low-mass, cool white dwarf plus a hotter and rather massive white dwarf that is rapidly rotating. While our paper was under review, Kulkarni & van Kerkwijk (2010) published an independent study of SDSSJ1257+5428, coming to broadly similar conclusions, but with noticeable differences in the detailed white dwarf parameters. In the light of this development, we re-visited the modelling of the WHT spectroscopy and the ultraviolet (UV)/optical spectral energy distribution (SED), adopting three different approaches which we now detail.

3.4.1. Disentangled spectra

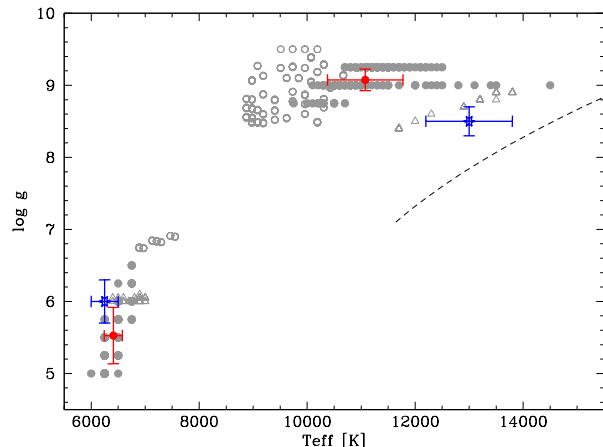


FIG. 6.— Constraints on the effective temperatures and surface gravities of the two white dwarfs in SDSSJ1257+5428. Fits to the disentangled spectra (Sect. 3.4.1) were carried out with light ratios 0.7–1.3 in steps of 0.1, and secondary star rotation rates $v \sin i = 500 - 1750 \text{ km s}^{-1}$ in steps of 250 km s^{-1} , and are shown as open circles. The best-fit parameters from fitting the phase-resolved 2009 WHT spectroscopy (Sect. 3.4.2) are shown as filled circles, their averages and standard deviations are indicated by the red error bars ($T_{1,\text{eff}} = 6341 \pm 139 \text{ K}$, $\log g_1 = 5.40 \pm 0.37$, $T_{2,\text{eff}} = 11111 \pm 704 \text{ K}$, and $\log g_2 = 9.13 \pm 0.14$). Fits to the SDSS/UVOT broad-band photometry are shown as triangles (Sect. 3.4.3). The blue error bars show the best-fit parameters of Kulkarni & van Kerkwijk (2010), and the dashed line indicates the occurrence of maximum Balmer-line strength.

TABLE 1
SUMMARY OF EFFECTIVE TEMPERATURE AND GRAVITY
MEASUREMENTS FOR SDSSJ1257+5428.

Source	$T_{\text{eff},1}$ [K]	$\log g_1$ [cm s^{-2}]	$T_{\text{eff},2}$ [K]	$\log g_2$ [cm s^{-2}]
Disentangling	7200 ± 350	6.9 ± 0.1	9800 ± 1000	9.0 ± 0.4
Phase-resolved	6340 ± 140	5.4 ± 0.4	11100 ± 710	9.1 ± 0.2
UV-optical SED	6620 ± 200	6.1 ± 0.1^a	12400 ± 710	8.6 ± 0.2
KvK2010	6250 ± 250	6.0 ± 0.3^a	13000 ± 800	8.5 ± 0.2

^aFits limited to $\log g > 6.0$.

We modelled the two individual spectral components resulting from the disentangling of Fig. 4 using the fitting routine of Rebassa-Mansergas et al. (2007). The grid of DA model spectra which was calculated as in Koester et al. (2005), includes the updated Stark broadening of the Balmer lines of Tremblay & Bergeron (2009), and spans $5 < \log g < 9.5$ in steps of 0.25 and 131 temperatures sampling the range $6000 < T_{\text{eff}} < 100000 \text{ K}$ in an optimised way.

Given that the relative flux ratio of the disentangled components is indeterminate, we carried out fits adopting a range of “light ratios”, $l = 0.7 - 1.3$ (in steps of 0.1), defined such that the secondary star contributes l while the primary contributes $2 - l$ to the observed light. Changing the light ratio modifies the ratio of the Balmer line equivalent widths between the two components, and light ratios outside the adopted range resulted in unphysical line strengths for one or both components. In addition, while spectral disentangling adopts a single value for the light ratio across the entire spectral range that is analysed, the true light ratio of the two white dwarfs in SDSSJ1257+5428 is a function of the wavelength. This may introduce systematic uncertainties (see Sect. 3.4.2), although one would hope that the range of light ratios

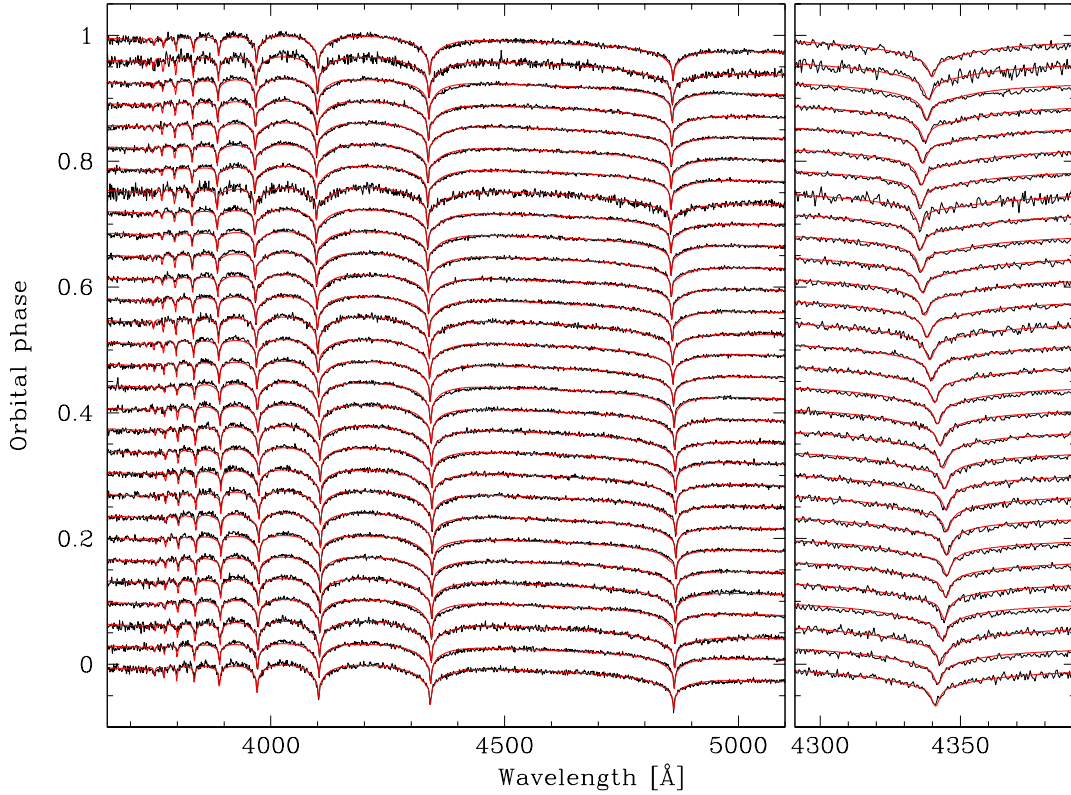


FIG. 7.— Composite model fits (red) to the 2009 WHT spectroscopy of SDSSJ1257+5428, averaged in 30 orbital phase bins (black). Each individual spectrum was fitted independently, resulting in 30 solutions for $T_{1,\text{eff}}$, $\log g_1$, $T_{2,\text{eff}}$, $\log g_2$ (see Fig. 6), and the relative flux contribution of both white dwarfs.

adopted would reveal such systematics through variation in the best fit parameters. Conditions during our observations precluded any reliable flux calibration of our spectra and we use no information from the continuum. For each assumed light ratio l , the model fit to the primary results in a best-fit effective temperature and surface gravity, an example for $l = 0.7$ is shown in Fig. 4. Figure 6 illustrates that regardless of l , the parameters of the primary are constrained within a narrow range, $T_{\text{eff},1} = 7200 \pm 350$ K and $\log g_1 = 6.85 \pm 0.10$. This temperature and gravity implies a very low mass for the primary, $M_1 = 0.20 \pm 0.05 M_\odot$ (Panei et al. 2007). These fit parameters and others discussed in this paper, including those of Kulkarni & van Kerkwijk (2010) listed as KvK2010, are summarised in Table 1.

The broad Balmer lines of the secondary (particularly $H\alpha$) suggest rapid rotation. Assuming this, we found that acceptable fits were only obtained for projected equatorial rotation speeds in the range $v \sin i = 500 - 1750 \text{ km s}^{-1}$. The distributions of the best-fit parameters in the $T_{\text{eff}} - \log g$ plane are again illustrated in Fig. 6, with higher values of $v \sin i$ requiring lower $\log g$ to reproduce the observed broad line profiles. These span a range $T_{\text{eff},2} = 9800 \pm 1000$ K and $\log g_2 = 9.0 \pm 0.4$, corresponding to $M_2 = 1.2 \pm 0.2 M_\odot$, consistent with the kinematic constraints of Fig. 8. These parameters broadly agree with the findings of Kulkarni & van Kerkwijk (2010), however, they found an even lower gravity for the low-mass white dwarf primary ($\log g_1 = 6.0 \pm 0.3$), and a higher temperature for the more massive secondary ($T_{\text{eff},2} = 13000 \pm 800$ K). We will see below, as is

also clear from Table 1, that the *Swift* UVOT fluxes of SDSSJ1257+5428 (section 3.4.3) indeed suggest that $T_{\text{eff},2}$ from modelling the disentangled spectra is too low.

3.4.2. Phase-binned flux spectra

An assumption inherent to the spectral disentangling is a constant light ratio, i.e. relative flux contribution of both components, across the wavelength range under analysis. Our application of the method over the entire wavelength range of the blue WHT spectra violates this assumption, which will result in systematic errors in the relative strengths of the individual Balmer lines, although as we remarked, our use of a range of light ratios might be expected to transfer any resulting variation into the final uncertainties. However, as an alternative we decided to carry out more direct fits to the WHT spectra. We binned the 118 individual spectra into 30 phase bins, and fitted each of them separately with the sum of two white dwarf model spectra drawn from the same model grids as in Sect. 3.4.1. Observed and model spectra were normalised prior to the fits. The fits were repeated for a range of rotational velocities for the more massive white dwarf, $500 < v \sin i < 1750 \text{ km s}^{-1}$, in steps of 250 km s^{-1} .

Figure 7 shows the independent best-fits to the 30 phase-binned spectra for $v \sin i = 1000 \text{ km/s}$. The distributions of the 30 individual best-fit white dwarf parameters are shown in Fig. 6. Each of the 30 independent fits leads to a pair of points in this figure, one in each of the two separate groups of points. Averaging these groups leads to $T_{\text{eff},1} = 6340 \pm 140$ K, $\log g_1 = 5.40 \pm 0.37$,

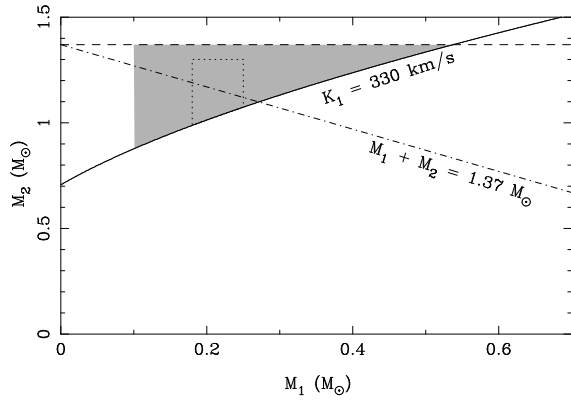


FIG. 8.— Constraints upon the masses of the two stars in SDSSJ1257+5428. The solid curved line is the lower limit upon M_2 given $K_1 = 330 \text{ km s}^{-1}$. The value of M_2 is bounded from above by the Chandrasekhar limit (horizontal dashed line), $M_{\text{Ch}} = 1.37 M_{\odot}$, while a conservative minimum white dwarf mass of $0.1 M_{\odot}$ places a lower limit upon M_1 . These three constraints lead to the shaded triangular region. The dotted-line box outlines the more arguable region of parameter space favored by the spectroscopic and evolutionary arguments outlined in section 4.1.

$T_{\text{eff},2} = 11100 \pm 710 \text{ K}$, and $\log g_2 = 9.13 \pm 0.14$. Higher (lower) values for $v \sin i$ shifts both white dwarfs to lower (higher) T_{eff} and $\log g$, by a few hundred degrees and 0.1–0.2 dex, with no significant difference in the quality of the fits.

Compared to the fit of the disentangled spectra (Sect. 3.4.1), the two white dwarfs move further apart in the $(T_{\text{eff}}, \log g)$ plane, somewhat in the sense of Kulkarni & van Kerkwijk (2010). Interestingly, $\log g_1 = 5.40 \pm 0.37$ from fitting the phase-binned spectra is even lower than that reported by Kulkarni & van Kerkwijk (2010), $\log g_1 = 6.0 \pm 0.3$. However, their best-fit value for $\log g_1$ is on the boundary of their model grid, and thus may have been limited by the range of their models. This exceedingly low gravity by white dwarf standards raises evolutionary problems as we elucidate in section 4.1.

The best-fit parameters show considerable scatter in the gravity of the primary, $\log g_1$ and the temperature of the secondary, $T_{\text{eff},2}$, which are poorly constrained by the standards of single white dwarf spectra of comparable quality. Presumably the simultaneous fit of two spectra introduces an element of degeneracy not present for single white dwarfs.

3.4.3. SDSS and UVOT spectral energy distribution

At optical wavelengths the cool, low-mass primary dominates the observed flux of SDSSJ1257+5428. However, given the substantial difference in effective temperatures, the flux contribution of the two white dwarfs is expected to reverse in the ultraviolet, which motivated our *Swift* TOO observations. These show an increasing flux towards shorter wavelengths (Fig. 9). We have fitted the energy distribution spanned by the broad-band fluxes in the UVOT uvw2, uvm2, uvw1, and b-bands and in the SDSS *ugriz*-bands with composite white dwarf models, using the same model grid as in Sect. 3.4.1 and 3.4.2. More specifically, we fold all model spectra through the spectral response curves of the *Swift* and SDSS bandpasses, and calculate absolute magnitudes

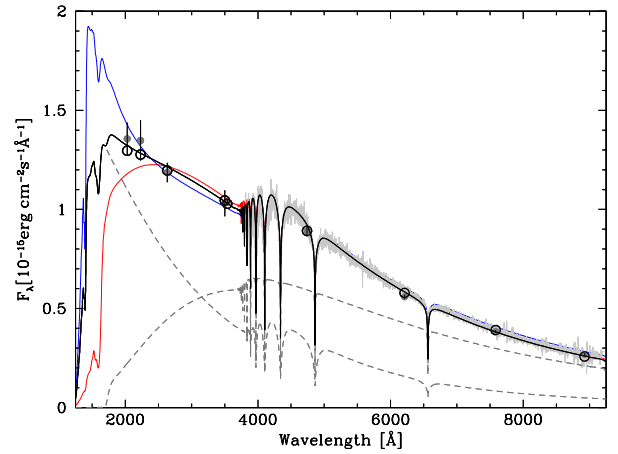


FIG. 9.— The spectral energy distribution of SDSSJ1257+5428. SDSS and UVOT broad-band fluxes are shown as filled circles, also plotted is the SDSS spectrum (gray). The best-fit to the broad-band fluxes is shown by the solid black line (middle in the FUV), with the individual contributions of the cool and hot components by dashed gray lines. A composite model for the parameters of Kulkarni & van Kerkwijk (2010) is shown in blue (highest in the FUV); our best fit to the phase-dependent WHT spectra (Sect. 3.4.2, Fig. 7) in red (lowest in the FUV).

using the cooling sequences of Bergeron et al. (1995)¹, which we extrapolated down to $\log g = 6.0$. In a final step, the co-added set of absolute magnitudes are fitted to the *Swift* and SDSS data. The best fit formally gives $T_{1,\text{eff}} = 6620 \pm 200 \text{ K}$, $\log g_1 = 6.1 \pm 0.1$, $T_{2,\text{eff}} = 12400 \pm 400 \text{ K}$, and $\log g_2 = 8.6 \pm 0.2$, which are similar to those of Kulkarni & van Kerkwijk (2010), but suffer from the same limitation, namely being hard-bounded at $\log g = 6.0$, in our case by the cooling sequences we used. Nevertheless, the UVOT fluxes clearly favor a temperature for the secondary at the high end of the values returned by our spectroscopic fits.

Figure 9 illustrates our average best-fit to the phase-binned spectra, the fit to the UV/optical broad-band fluxes, and a model computed using the parameters of Table 1 in Kulkarni & van Kerkwijk (2010) along with the *Swift* and SDSS broad-band fluxes, and the SDSS spectrum. The parameters used in the models are those summarised in Table 1. The models diverge in the far ultraviolet and will be easily distinguishable with *HST* spectra. The model based upon the mean of our phase-binned data is too cool, while that based upon Kulkarni & van Kerkwijk (2010) is a little too hot in the FUV and too cool at optical wavelengths. The temperature of the secondary from the disentangled spectra (9800 K) is obviously much too cool and we plot no corresponding SED in Fig. 9.

In summary, the optical and ultraviolet characteristics of SDSSJ1257+5428 are consistent with a double-degenerate consisting of a cool, extremely low-mass white dwarf plus a rather massive, hotter white dwarf. We estimate the distance to the binary to be $d \sim 100 \text{ pc}$, larger than the 48 pc estimated by Badenes et al. (2009) because of the larger size of the primary. However, the data currently available are insufficient to fully constrain the five free parameters ($T_{1,\text{eff}}$, $\log g_1$, $T_{2,\text{eff}}$, $\log g_2$ and $v \sin i$).

¹ An updated 2006 version is available at <http://www.astro.umontreal.ca/~bergeron/CoolingModels>

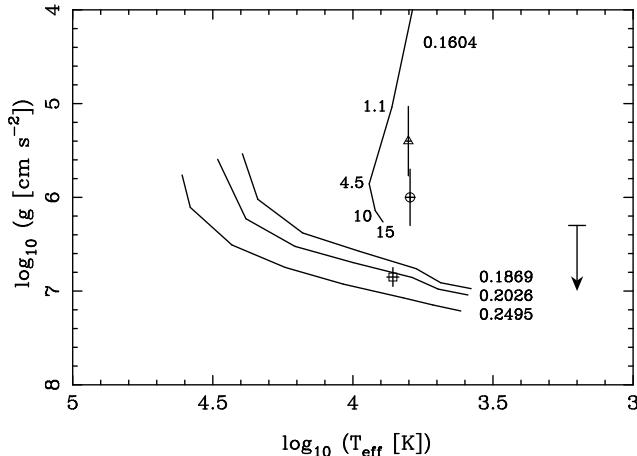


FIG. 10.— From top to bottom the symbols with error bars show the temperature and gravity of the low-mass primary based upon (i) our phase-resolved spectra (triangle), (ii) Kulkarni & van Kerkwijk (2010)’s equivalent result (circle), and (iii) our fit to the disentangled spectra (square). The lines show evolutionary models for different mass helium white dwarfs from Panei et al. (2007). The cooling ages in Gyr are labelled on the $0.1604 M_{\odot}$ model which is slowed by hydrogen fusion. The arrow in the lower right indicates the lower limit on gravity based upon assuming that the secondary contributes at least 25% of the flux.

4. DISCUSSION

4.1. Present state of SDSSJ1257+5428

The precise nature of the low mass primary star in SDSSJ1257+5428 presents us with a puzzle. As Fig. 10 shows, the fits to the disentangled spectra are consistent with a mass of around $0.2 M_{\odot}$ (Panei et al. 2007). The cooling age in this case is ~ 1 Gyr which just about allows the secondary star (cooling age 1 to 2 Gyr, for CO and ONe models (Bergeron et al. 1995; Althaus et al. 2007)) to have a longer cooling age than the primary, as we expect, since the massive white dwarf presumably formed before the helium white dwarf. In contrast, our phase-resolved fits, which fit the data directly, as well as the similar fits of Kulkarni & van Kerkwijk (2010), suggest a much lower gravity and a mass $< 0.16 M_{\odot}$. In fact, as both Figs 6 and 10 show, the gravity of the primary is very poorly constrained by the spectroscopic fits, ranging from $\log g = 5$ to 6.6 (and even then the lower bound is set by the model grid). Crucially, this range allows the primary star to sit on either side of the division at $\sim 0.18 M_{\odot}$ below which residual hydrogen on the surface of helium white dwarfs can maintain fusion and greatly slow their cooling whereas above, hydrogen shell flashes can remove the hydrogen and allow normal cooling (Kippenhahn et al. 1968; Webbink 1975; Driebe et al. 1998; Sarna et al. 2000; Althaus et al. 2001; Nelson et al. 2004; Panei et al. 2007). As Fig. 10 shows, if the mass of the primary is below this limit, then in order to keep the cooling age of the primary short enough to allow the secondary to be as hot as it is, the gravity must lie at the lower end of the range with $\log g \approx 5$.

Such a low gravity is hard to believe because, for reasonable assumptions about the masses of the two stars, the primary becomes so large that it drowns out the light from the secondary. Quantitatively, the ratio r of the flux from the secondary divided by that from the

primary, at wavelength λ is given by

$$r = \frac{R_2^2 F(\lambda, T_2)}{R_1^2 F(\lambda, T_1)}, \quad (2)$$

where F is the astrophysical flux density (flux per unit wavelength per unit area of the star). Using $R^2 \propto M/g$ and applying the observed 3:1 maximum ratio (from the disentangling light ratio limits) gives therefore

$$r = \frac{M_2 g_1 F(\lambda, T_2)}{M_1 g_2 F(\lambda, T_1)} > \frac{1}{3}. \quad (3)$$

This then leads to a lower limit upon the gravity of the primary:

$$g_1 > \frac{1}{3} \frac{M_1 g_2 F(\lambda, T_1)}{M_2 F(\lambda, T_2)}. \quad (4)$$

Assuming $M_2 = 1.0 M_{\odot}$, $\log g_2 = 8.64$, $M_1 = 0.15$ (a lower limit to give the least stringent constraint on g_1), $T_1 = 6300$, $T_2 = 14000$ K (an upper limit, again to give the weakest constraint on g_1), and taking the ratio of model atmospheres at $\lambda = 483$ nm (g -band central wavelength), we find $\log g_1 > 6.3$. We plot this lower limit on the right-hand side of Fig. 10. This limit suggests that the surface gravity of the primary star is at the upper end of the range returned by the spectroscopic fits. If the primary has a mass below $0.18 M_{\odot}$, as the spectroscopic fits seem to favour, then the evolutionary models suggest that its cooling age is of order 10 Gyr.

We are left with a choice between two unpalatable alternatives: either the primary has a mass above $> 0.18 M_{\odot}$, as suggested by the fits to the disentangled spectra but in contradiction with both our direct fits and those of Kulkarni & van Kerkwijk (2010), or it has a mass below this limit and is therefore extremely old, making the youth of the more massive secondary impossible to understand, since it should have formed first.

We do not have a satisfactory resolution of this problem, but marginally prefer the higher mass solution ($M_1 \sim 0.2 M_{\odot}$) for the primary to avoid the relative age problem. This supposes that the evolutionary models are correct; further work to fix M_1 is encouraged. If we are right that the primary mass in SDSSJ1257+5428 is $0.2 M_{\odot}$, then the mass of the secondary is $> 1 M_{\odot}$ (Fig. 8). This puts the secondary close to the dividing line between CO and ONe white dwarfs which is thought to lie at around $1.05 M_{\odot}$ for solar metallicity progenitors, corresponding to an initial mass of about $5.5 M_{\odot}$ (Meng et al. 2008).

We suspect that the discrepancies in the best-fit parameters between the various fits result from difficulties in establishing reliable continua given the extremely broad wings from the high mass white dwarf and, in our case at least, wavelength dependent slit losses during the rather poor conditions of our observing run. Differences between the model atmospheres and data are visible in both Figs 4 and 7. As a result, our best-fit parameters suffer from some systematic errors, which are only compounded by the degeneracy from fitting two spectra. The independent evidence provided by the UV-optical SED favors a high temperature for the secondary as found by Kulkarni & van Kerkwijk (2010), suggesting that their data are less affected by continuum problems than ours,

although their low gravity for the primary possibly indicates that they are not entirely immune to the same problems. Further observations are needed to clarify this issue.

4.2. Anomalous broadening

Although there has been debate over the first phase of mass transfer in the formation of double white dwarfs, the second phase, involving mass transfer onto the white dwarf that forms first, is almost universally assumed to lead to the formation of a common envelope (Han 1998; Nelemans et al. 2001b). However, the absence of a narrow core in $H\alpha$ of the secondary white dwarf in SDSSJ1257+5428 is suggestive of rapid rotation with $v \sin i > 500 \text{ km s}^{-1}$, which throws doubt upon this assumption since we estimate from consideration of the moment of inertia of the white dwarf and the angular momentum of the accreted material that it should have accreted $> 0.02 M_{\odot}$ to attain this rotation rate. This would require a much more prolonged period of accretion than allowed by a common envelope, given a maximum accretion rate onto a white dwarf of a few $\times 10^{-7} M_{\odot} \text{ yr}^{-1}$ (Nomoto et al. 2007). This is reminiscent of evolutionary scenarios involving stable second phases of mass transfer discussed by Sarna et al. (1996). A possible near-relative of SDSSJ1257+5428 is the star HD 49798 in which a massive, rapidly spinning white dwarf orbits an sdO star (Mereghetti et al. 2009). Uncertainty remains however over the cause of the broad profiles. There is no sign of Zeeman splitting in $H\alpha$ (Fig. 5), but as Kulkarni & van Kerkwijk (2010) suggest, a magnetic field could make the core more difficult to see, and, if suitably distributed in strength across the surface, would not necessarily lead to obvious splitting. In a dual rotation-plus-magnetic-field model, the field could also act to increase the lever arm for accretion and hence reduce the amount of material needed to spin the white dwarf up. Alternatively, if the atmosphere is helium-dominated, we will see deeper into the star which may allow Stark broadening to wipe out the $H\alpha$ core. Finally, the temperature of the secondary star is such that it could lie within the ZZ Ceti pulsational instability strip. It is observed (Koester et al. 1998) that ZZ Ceti stars show weak cores in $H\alpha$, probably the result of motion in their photospheres (Koester & Kompas 2007). It would be worth observing SDSSJ1257+5428 photometrically for pulsations.

4.3. Future evolution

Close pairs of white dwarfs are common within our Galaxy, and their future evolution has been the subject of much discussion, not least as potential progenitors of

Type Ia supernovae. For SDSSJ1257+5428, the first step is clear: gravitational radiation will reduce the orbital period to the point at which mass transfer starts. The orbital period at this point will be about 1.5 minutes which will be reached in $\sim 3 \times 10^9$ years. The outcome of mass transfer is uncertain and our constraints allow any of three possibilities which are (i) explosion as a Type Ia supernova, (ii) accretion-induced collapse to a millisecond pulsar and (iii) survival of the onset of mass transfer as a hydrogen-deficient ultra-compact binary. We slightly favor the third possibility on the grounds that the mass ratio $q = M_1/M_2 \approx 0.2$ is extreme enough to allow stable mass transfer (Nelemans et al. 2001a; Marsh et al. 2004), while we suspect the total mass to be less than the Chandrasekhar mass. SDSSJ1257+5428 is therefore likely to become a semi-detached, accreting double white dwarf (AM CVn star). The secondary star will become the accretor. Since it is massive for a white dwarf, and as long as it is not an ONe white dwarf, the system is a good candidate progenitor of the sub-luminous “Ia” supernovae discussed by Bildsten et al. (2007) and possibly observed by Kasliwal et al. (2010).

5. CONCLUSION

We find that the putative white dwarf-black-hole/neutron star binary, SDSSJ1257+5428, is a double white dwarf. SDSSJ1257+5428 is composed of a very low mass $\sim 0.2 M_{\odot}$ white dwarf together with an extremely massive ($> 1 M_{\odot}$) white dwarf. As long as the massive white dwarf avoids accretion-induced collapse or explosion, SDSSJ1257+5428 will evolve into a hydrogen-deficient accreting binary star, but may later explode as a sub-luminous Type Ia. The massive white dwarf shows signs of rapid rotation ($v \sin i > 500 \text{ km s}^{-1}$) which suggests that the most recent phase of mass transfer might not have involved a common envelope, contrary to current models of double white dwarf populations. Some inconsistencies in the parameters of the two white dwarfs remain that are probably caused by difficulties in fitting their blended spectra; further observations are required to clarify these.

We thank Sergio Campana for the use of his additional *Swift* data. We made use of SIMBAD, maintained by the Centre Données astronomiques de Strasbourg and the National Aeronautics and Space Administration’s Astrophysics Data System. TRM, BTG, DS and JS acknowledge the financial support of the UK’s STFC. Balmer/Lyman lines in the models were calculated with the modified Stark broadening profiles of Tremblay & Bergeron (2009) kindly made available by the authors.

REFERENCES

- Althaus, L. G., García-Berro, E., Isern, J., Córscico, A. H., & Rohrmann, R. D. 2007, *A&A*, 465, 249
- Althaus, L. G., Serenelli, A. M., & Benvenuto, O. G. 2001, *MNRAS*, 324, 617
- Badenes, C., Mullally, F., Thompson, S. E., & Lupton, R. H. 2009, *ApJ*, 707, 971
- Bergeron, P., Wesemael, F., & Beauchamp, A. 1995, *PASP*, 107, 1047
- Bildsten, L., Shen, K. J., Weinberg, N. N., & Nelemans, G. 2007, *ApJ*, 662, L95
- Bragaglia, A., Greggio, L., Renzini, A., & D’Odorico, S. 1990, *ApJ*, 365, L13
- Driebe, T., Schoenberner, D., Bloeker, T., & Herwig, F. 1998, *A&A*, 339, 123
- Eisenstein, D. J., Liebert, J., Harris, H. C., Kleinman, S. J., Nitta, A., Silvestri, N., Anderson, S. A., Barentine, J. C., Brewington, H. J., Brinkmann, J., Harvanek, M., Krzesiński, J., Neilsen, Jr., E. H., Long, D., Schneider, D. P., & Snedden, S. A. 2006, *ApJS*, 167, 40
- Greenstein, J. L. & Peterson, D. M. 1973, *A&A*, 25, 29

- Han, Z. 1998, MNRAS, 296, 1019
- Heber, U., Napiwotzki, R., & Reid, I. N. 1997, A&A, 323, 819
- Horne, K. 1986, PASP, 98, 609
- Iben, Jr., I. & Tutukov, A. V. 1984, ApJS, 54, 335
- Kasliwal, M. M., Kulkarni, S. R., Gal-Yam, A., Yaron, O., Quimby, R. M., Ofek, E. O., Nugent, P., Poznanski, D., Jacobsen, J., Sternberg, A., Arcavi, I., Howell, D. A., Sullivan, M., Rich, D. J., Burke, P. F., Brimacombe, J., Milisavljevic, D., Fesen, R., Bildsten, L., Shen, K., Cenko, S. B., Bloom, J. S., Hsiao, E., Law, N. M., Gehrels, N., Immler, S., Dekany, R., Rahmer, G., Hale, D., Smith, R., Zolkower, J., Velur, V., Walters, R., Henning, J., Bui, K., & McKenna, D. 2010, ApJ, 723, L98
- Kippenhahn, R., Thomas, H., & Weigert, A. 1968, ZAp, 69, 265
- Koester, D., Dreizler, S., Weidemann, V., & Allard, N. F. 1998, A&A, 338, 612
- Koester, D. & Herrero, A. 1988, ApJ, 332, 910
- Koester, D. & Kompas, E. 2007, A&A, 473, 239
- Koester, D., Napiwotzki, R., Voss, B., Homeier, D., & Reimers, D. 2005, A&A, 439, 317
- Kulkarni, S. R. & van Kerkwijk, M. H. 2010, ApJ, 719, 1123
- Marsh, T. R. 1989, PASP, 101, 1032
- Marsh, T. R., Dhillon, V. S., & Duck, S. R. 1995, MNRAS, 275, 828
- Marsh, T. R., Nelemans, G., & Steeghs, D. 2004, MNRAS, 350, 113
- Meng, X., Chen, X., & Han, Z. 2008, A&A, 487, 625
- Mereghetti, S., Tiengo, A., Esposito, P., La Palombara, N., Israel, G. L., & Stella, L. 2009, Science, 325, 1222
- Napiwotzki, R., Drechsel, H., Heber, U., Karl, C., Pauli, E.-M., Christlieb, N., Hagen, H.-J., Reimers, D., Koester, D., Moehler, S., Homeier, D., Leibundgut, B., Renzini, A., Marsh, T. R., Nelemans, G., & Yungelson, L. 2003, in NATO ASI Proc. 105: White Dwarfs, 39
- Nelemans, G., Portegies Zwart, S. F., Verbunt, F., & Yungelson, L. R. 2001a, A&A, 368, 939
- Nelemans, G., Yungelson, L. R., Portegies Zwart, S. F., & Verbunt, F. 2001b, A&A, 365, 491
- Nelson, L. A., Dubeau, E., & MacCannell, K. A. 2004, ApJ, 616, 1124
- Nomoto, K., Saio, H., Kato, M., & Hachisu, I. 2007, ApJ, 663, 1269
- Panei, J. A., Althaus, L. G., Chen, X., & Han, Z. 2007, MNRAS, 382, 779
- Rebassa-Mansergas, A., Gänsicke, B. T., Rodríguez-Gil, P., Schreiber, M. R., & Koester, D. 2007, MNRAS, 382, 1377
- Robinson, E. L. & Shafter, A. W. 1987, ApJ, 322, 296
- Roming, P. W. A., Kennedy, T. E., Mason, K. O., Nousek, J. A., Ahr, L., Bingham, R. E., Broos, P. S., Carter, M. J., Hancock, B. K., Huckle, H. E., Hunsberger, S. D., Kawakami, H., Killough, R., Koch, T. S., McLelland, M. K., Smith, K., Smith, P. J., Soto, J. C., Boyd, P. T., Breeveld, A. A., Holland, S. T., Ivanushkina, M., Pryzby, M. S., Still, M. D., & Stock, J. 2005, Space Science Reviews, 120, 95
- Sarna, M. J., Ergma, E., & Gerškevič-Antipova, J. 2000, MNRAS, 316, 84
- Sarna, M. J., Marks, P. B., & Connors Smith, R. 1996, MNRAS, 279, 88
- Simon, K. P. & Sturm, E. 1994, A&A, 281, 286
- Tremblay, P.-E. & Bergeron, P. 2009, ApJ, 696, 1755
- Webbink, R. F. 1975, MNRAS, 171, 555
- . 1984, ApJ, 277, 355